Lock-release gravity currents and dam-break flows

By ANDREW J. HOGG

Centre for Environmental and Geophysical Flows, School of Mathematics,
University of Bristol, Bristol BS8 1TW, UK
a.j.hogg@bris.ac.uk

Gravity current and dam-break flows, resulting from the instantaneous release of fluid initially at rest behind a lock gate, are modelled theoretically using the shallow water equations. By analysing the motion in the hodograph plane, the governing equations become linear and hence it is possible to integrate them analytically from lock-release initial conditions. This approach provides many advantages: not only are numerical computations obviated, but the analysis clearly reveals how the nature of the ensuing flow depends on the Froude number, Fr, at the front of the current. It is also demonstrated that the motion comprises uniform and simple wave regions within which both or one of the characteristic variables are constant, respectively, in addition to complex wave regions within which both characteristic variables vary. These solutions reveal phenomena that have not previously been reported for gravity current flow. Specifically, when $Fr > 2$, the height and velocity fields become discontinuous at late times at an interior point within the current. Conversely, when $Fr < 2$, there is a wave-like disturbance that propagates along the length of the current, being reflected successively between the rear wall of the lock and the front of the flow.

1. Introduction

The study of gravity currents, in which relatively dense fluid is introduced into less dense surroundings, and dam-break flows, in which initially stationary fluid is set into motion from behind a rapidly removed vertical lock-gate, has a long history (Ritter 1892; von Kármán 1940) and yet they are still a focus of much recent research, because many aspects of their motion remain incompletely understood. These flows are important to a wide range of industrial and environmental applications including the motion of the flood wave following the failure of a constructed dam, the spreading of relatively dense poisonous gas, the intrusion of saline water through estuaries and the run-up of bores and swash on beaches. Much of the fascination of these flows arises from the rich variety of dynamical behaviour that may be exhibited as they propagate over horizontal boundaries in an unsteady manner from their source, driven by their excess density.

There have been many theoretical advances in mathematical modelling of the motion. Simplest approaches employ dimensional reasoning and straightforward integral models to predict the flow speed as a function of the initial conditions (see, for example, Huppert & Simpson 1980; Hogg, Hallworth & Huppert 2005). More sophisticated approaches develop shallow-layer descriptions of the motion, based upon the thinness of the flows. These resolve some of the interior dynamics, but must be supplemented

by a semi-empirical dynamic condition at the front of the motion to represent the unsteady and three-dimensional flow that occurs there (Benjamin 1968; Rottman & Simpson 1983; Shin, Dalziel & Linden 2004). These shallow-layer models admit similarity solutions that provide the long-term asymptotics for the motion once the detailed initial structure of the height and velocity fields are no longer significant, save for their contribution to the overall buoyancy of the release (Fannelop & Waldman 1972; Hoult 1972; Mathunjwa & Hogg 2006). Finally, some recent investigations have succeeded in numerically simulating the motion by integrating more complete three-dimensional models of the motion, thus obviating the need for assumptions concerning the dominant length scales and dynamic balances within the flow, but at the cost of lengthy numerical computations (Härtel, Meiburg & Necker 2000).

Many experimental investigations of gravity currents and dam-break flows have instantaneously released fluid within a flume from behind a vertical lock gate (see, for example, Huppert & Simpson 1980; Rottman & Simpson 1983; Lauber & Hager 1998). In such experiments the gate is rapidly removed and these lock releases have proven to be a repeatable means for generating flows within the laboratory that are essentially two-dimensional. Furthermore, although somewhat idealized, such conditions provide an attractive initial configuration for theoretical considerations. Typically if resistive forces are negligible, two-dimensional lock-release gravity currents rapidly accelerate from rest to exhibit a regime in which the front moves at constant velocity, before decelerating and entering a self-similar regime in which the front position, x_N, depends upon the time from release to the $\frac{2}{3}$ power, $t^{2/3}$ (Rottman & Simpson 1983).

This paper provides a theoretical study of dam-break flows and of gravity currents generated by lock releases of relatively dense fluids. We adopt a shallow-layer model in which resistive forces are negligible and the motion arises from a balance between the streamwise pressure gradient and the inertia of the fluid. Our key contribution in this paper is to integrate the nonlinear governing equations analytically and elucidate the velocity and height fields for the entire motion at all times after the flow is initiated. This is made possible by adopting a hodograph transformation of the governing equations that converts the nonlinear system into a linear system. This means that rather than resorting to numerical computations of the hyperbolic governing partial differential equations, the flow may be calculated from relatively simple analytical expressions. Indeed, as described below, our analysis reveals features of the motion that have not been reported before. We note that the application of hodograph techniques to the shallow water equations is not new. For example Carrier & Greenspan (1957) employed the technique to construct nonlinear periodic waves on a plane beach and recently this was extended to more general wave forms by Carrier, Wu & Yeh (2003). Kerswell (2005) applied the technique to dam-break releases of cohesionless granular material. This latter contribution shares the same initial condition as the fluid flows analysed in this paper, but the boundary conditions are different. Also Kerswell (2005) showed that these granular flows are rapidly arrested by frictional forces, whereas fluid flows may propagate over large distances before being influenced by drag (Hogg & Pritchard 2004).

The hodograph technique applied in this study relies on the hyperbolic character of the governing equations and that there are two distinct characteristic directions. An important result is that we may readily find the characteristic curves and the regions within which the characteristic quantities take constant values (uniform and simple wave regions). This approach has been undertaken before for these types of flows: for dam-break flows from a lock of infinite extent, with the leading edge defined by vanishing flow depth, Ritter (1892) showed that the entire motion was

readily calculated in terms of a simple wave region; Abbott (1961) extended this for more general conditions at the front; and Rottman & Simpson (1983) showed that the characteristics reflect from the rear wall of the lock, propagate forward to catch up the front and generate regions where both characteristics values vary (complex wave region). They did not, however, explicitly calculate the characteristic curves, nor did they attempt to find the long-term behaviour within the complex wave regions using analytical methods. The flow structure shares some features with phenomena found in the motion of compressible gases. For example, Stanyukovich (1960) identifies regions of uniform flow, rarefactions (simple waves) and reflected waves when a gas, confined within a tube, is allowed to expand by removing a piston from one end. It should be noted, though, that the boundary condition on this gas flow at the piston differs from the dynamic condition at the front of gravity currents and this necessitates the use here of a rather different approach to calculate the flow. In this study we demonstrate how to compute the structure and form of the characteristic plane directly and we show how it depends upon the magnitude of the Froude number at the front of the flow, Fr, which measures the flow speed relative to the speed of infinitesimal long waves on the surface of the moving fluid. We note that when the current is propagating through sufficiently deep water, many investigators have found experimentally that the Froude number adopts a constant value; for example, Huppert & Simpson (1980) found that $Fr = 1.2$ for Boussinesq currents, while for the fronts of 'classical' dam-break flows of liquids through air the height vanishes and this corresponds to $Fr \to \infty$ (Whitham 1974). We will thus develop the solutions for the motion for all values of the frontal Froude number.

Our aims in this paper are two-fold. First we have constructed the complete solution for the flow analytically. This obviates the need for numerical calculations, which have had some difficulties in tracking accurately the motion of the front and in resolving regions where the height, velocity, or gradients of either of these, are discontinuous. The new analytical solutions therefore provide an important test-bed for future numerical codes designed to integrate the shallow water equations. However the analysis also reveals clearly how the dynamical behaviour depends on Fr and we find phenomena that have not been reported before. When $Fr < 2$ we find that a wave-like disturbance is generated that propagates along the entire current, being successively reflected between the rear wall and the front of the current. When $Fr > 2$ we reveal that at relatively late times after release the flow develops an interior shock over which the velocity and height fields are discontinuous, corresponding to a propagating bore or internal hydraulic jump.

The study is organized as follows. First we formulate the models and hodograph transformation that enable the subsequent analysis (§2). Next in §3, we analyse the initial motion both in terms of the characteristic curves and of the dependent variables. This indicates where the important features of the characteristic plane are to be found and reveals why the magnitude of the frontal Froude number is important in determining the motion. In §4, we complete the solution for the flow, treating separately the cases: (i) $Fr \to \infty$; (ii) $Fr = 2$; (iii) $Fr < 2$; and (iv) $Fr > 2$. Finally we summarize and draw some conclusions in §5 and draw out the connections between this analysis and the similarity solutions that provide the intermediate asymptotics for the motion.

2. Formulation

We analyse the two-dimensional motion of incompressible relatively dense fluid through a less dense surrounding ambient fluid, along a rigid horizontal boundary.

The streamwise length scale of the motion is assumed to be much greater than the depth of the intruding current, so that vertical fluid accelerations are negligible and the pressure is hydrostatic to leading order. With the further assumptions that resistive forces may be neglected and that the current does not mix with the ambient, the motion may be modelled by the shallow water equations (Whitham 1974). Thus aligning the x-axis with the direction of propagation and denoting the flow depth and velocity by h and u, respectively, we find that

$$\frac{\partial h}{\partial t} + \frac{\partial}{\partial x}(uh) = 0, \tag{2.1}$$

$$\frac{\partial u}{\partial t} + u\frac{\partial u}{\partial x} + g'\frac{\partial h}{\partial x} = 0, \tag{2.2}$$

where $g' = (\rho - \rho_a)g/\rho$ is the reduced gravity and ρ and ρ_a are the densities of the intruding and ambient fluids, respectively. These single-layer shallow water equations have been employed to model gravity current motion in a wide variety of contexts (see, for example, Hoult 1972; Rottman & Simpson 1983; Hallworth, Hogg & Huppert 1998), as well as wave and dam-break flows (see, for example, Peregrine 1972; Whitham 1974; Hogg & Pritchard 2004; Pritchard & Hogg 2005). We note that if the depth of the current is comparable with the depth of the ambient fluid through which it flows, then the motion of the ambient cannot be neglected. In this case two-layer shallow water equations may be formulated to model separately mass and streamwise momentum evolution within in each layer, while the pressure remains hydrostatic throughout the flow (see, for example, Rottman & Simpson 1983; Hogg *et al.* 2005 and Ungarish & Zemach 2005).

We investigate the motion from 'lock-release' initial conditions. These correspond to an initially stationary layer of dense fluid behind a vertical lock-gate, located at $x = x_0$, that is instantaneously removed at $t = 0$ to generate the flow. Such initial configurations are readily generated in the laboratory and have formed an important configuration for the experimental testing of the behaviour of the flows (Huppert & Simpson 1980; Rottman & Simpson 1983; Shin *et al.* 2004). Furthermore these are the initial conditions for dam-break flows, which are an important phenomenon in hydraulic engineering and which have formed an important test of numerical computations of the flow. These initial conditions are given by

$$h = h_0 \quad \text{and} \quad u = 0 \quad \text{for} \quad 0 \leqslant x \leqslant x_0. \tag{2.3}$$

Finally the model is completed by the specification of boundary conditions. At the rear of the lock there is an impermeable wall and thus

$$u = 0 \quad \text{at} \quad x = 0. \tag{2.4}$$

At the front of the current we impose a dynamic condition

$$u = Fr\left(g'h\right)^{1/2} \quad \text{at} \quad x = x_N(t), \tag{2.5}$$

where Fr is a constant, together with the condition of kinematic consistency that

$$u = \frac{\mathrm{d}x_N}{\mathrm{d}t} \quad \text{at} \quad x = x_N(t). \tag{2.6}$$

Expression (2.5) is termed the Froude number condition and demands that the ratio at the front of the current of the flow speed to the speed of infinitesimal long waves on the surface of the layer is constant. Such a condition is required because around the front of a gravity current there may be significant vertical fluid motions

and so the shallow-water description is no longer appropriate. The Froude number condition has been studied theoretically by Benjamin (1968) and Shin *et al.* (2004) and experimentally by a number of investigators including Huppert & Simpson (1980), Grobelbauer, Fannelop & Britter (1993), Shin *et al.* (2004) and Lowe, Rottman & Linden (2004). Most generally the Froude number is a function of the depth of the current relative to the depth of the ambient. When the ambient is much deeper than the current, the Froude number adopts a constant value which Huppert & Simpson (1980) measured experimentally to be 1.2 for flows in which the density difference between the fluids is small. For non-Boussinesq flows, Grobelbauer *et al.* (1993) and Lowe *et al.* (2004) have shown that the Froude number may take larger values and for flows of liquid through air, such as 'classical' dam-break flow, the front is usually identified as the position where $h = 0$ (Whitham 1974). This is equivalent to $Fr \to \infty$. In this study we will investigate the motion that occurs when Fr is constant and we elucidate the different behaviours that occur for different values of Fr.

At this stage it is convenient to adopt dimensionless variables, scaling the height of the current by h_0, the x-coordinate by x_0, the velocity by $(g'h_0)^{1/2}$ and the time by $x_0/(g'h_0)^{1/2}$. Henceforth all variables are assumed to have been rendered dimensionless according to these scales.

The system of hyperbolic governing equations (2.1)–(2.2) may be written in characteristic form (Whitham 1974). Denoting the characteristic variables by

$$\alpha = u + 2c, \qquad \beta = u - 2c, \tag{2.7}$$

where $c = \sqrt{h}$, the system is given by

$$\frac{d\alpha}{dt} = 0 \qquad \text{on} \qquad \frac{dx}{dt} = u + c, \tag{2.8}$$

$$\frac{d\beta}{dt} = 0 \qquad \text{on} \qquad \frac{dx}{dt} = u - c. \tag{2.9}$$

Thus we deduce that the faster of the forward propagating characteristics with speed $u + c$ catch up with the front which has speed $Fr\,c$ for all finite values of the Froude number. This effect has been employed by some schemes for the numerical integration of the governing equations to impose the boundary condition at the front of the current (Bonnecaze, Huppert & Lister 1993; Hallworth *et al.* 1998). In the limit $Fr \to \infty$, we note that the trajectory of the front corresponds to the leading characteristic.

In subsequent sections of this study, it is convenient to adopt hodograph variables. Under this approach, x and t are treated as dependent variables that are functions of the independent variables α and β. The characteristic form of the governing equation then becomes

$$\frac{\partial x}{\partial \beta} = \tfrac{1}{4}(3\alpha + \beta)\frac{\partial t}{\partial \beta} \qquad \text{on} \qquad \alpha = \text{constant}, \tag{2.10}$$

$$\frac{\partial x}{\partial \alpha} = \tfrac{1}{4}(\alpha + 3\beta)\frac{\partial t}{\partial \alpha} \qquad \text{on} \qquad \beta = \text{constant}. \tag{2.11}$$

This hodograph remains invertible provided the Jacobian, J, given by

$$J = \frac{\partial x}{\partial \alpha}\frac{\partial t}{\partial \beta} - \frac{\partial x}{\partial \beta}\frac{\partial t}{\partial \alpha}, \tag{2.12}$$

is finite and non-zero. Importantly the transformation becomes non-invertible in 'simple wave' and 'uniform' regions, within which one, or both, of the characteristics

take a constant value, respectively. Combining the hodograph equations, we find a single equation for $t(\alpha, \beta)$ given by

$$\frac{\partial^2 t}{\partial \alpha \partial \beta} = \frac{3}{2(\alpha - \beta)} \left(\frac{\partial t}{\partial \alpha} - \frac{\partial t}{\partial \beta} \right). \tag{2.13}$$

Thus we note that the hodograph transformation has yielded a linear governing equation, and that this linearity can be exploited to find solutions of the nonlinear shallow water equations (see, for example, Carrier & Greenspan 1957 and Carrier *et al.* 2003). We may also transform the boundary conditions into the hodograph plane. First the condition of no flow at rear of the lock (2.4) is given by

$$x = 0 \qquad \text{on} \qquad \alpha + \beta = 0. \tag{2.14}$$

The Froude number condition (2.5) is given by

$$\frac{\mathrm{d}x_N}{\mathrm{d}t} = \tfrac{1}{2}(\alpha + \beta) \qquad \text{on} \qquad \beta = -\lambda \alpha, \tag{2.15}$$

where $\lambda = (2 - Fr)/(2 + Fr)$. Treating the front position and the time at the front, t_N, as functions of the characteristic variables, the condition (2.15) may be rewritten to give

$$\frac{\partial x_N}{\partial \alpha} - \lambda \frac{\partial x_N}{\partial \beta} = \tfrac{1}{2}\alpha(1 - \lambda) \left(\frac{\partial t_N}{\partial \alpha} - \lambda \frac{\partial t_N}{\partial \beta} \right). \tag{2.16}$$

Finally we note that provided there are non-trivial characteristics, this yields

$$\alpha(1 + \lambda) \left(\frac{\partial t_N}{\partial \alpha} + \lambda \frac{\partial t_N}{\partial \beta} \right) = 0. \tag{2.17}$$

Rather than impose the condition of no flow at the rear of the lock (2.14), we find that it is simpler to treat the problem as symmetric around the line $\alpha + \beta = 0$. Thus we effectively consider back-to-back lock-releases, propagating in opposite directions. This ensures that $u = 0$ at $x = 0$ and then the solution domain within the hodograph plane is given by $\{(\alpha, \beta) : \beta + \lambda \alpha \leqslant 0; \alpha + \lambda \beta \geqslant 0\}$. This approach does not artificially restrict the solutions that we construct, because if $u = 0$ at $x = 0$, then from (2.2) $\partial h/\partial x = 0$. Thus solutions are continuously differentiable at $x = 0$.

Along α-characteristics, $\mathrm{d}x/\mathrm{d}t > 0$ for all values of α and β. Thus characteristic data are always propagated along these curves from the rear to the front of the current. Along β-characteristics $\mathrm{d}x/\mathrm{d}t = (\alpha + 3\beta)/4$ and so if $\alpha < -3\beta$ then it is possible for the direction of characteristic data propagation to be reversed. However if $\beta > 0$ then there is no position within the current where this may occur because α is always positive. At the front of the current, $\beta = -\lambda \alpha$, and so we observe that if $Fr > 2$ then $\lambda < 0$ and this implies that β at the front is positive. This means that for $Fr > 2$ we do not expect the motion of the front to influence the dynamics at the rear of the current. Conversely if $Fr < 2$ then we may find β-characteristics that propagate from front to rear and there is the possibility for a wave-like disturbance to travel along the current, being reflected at the front and at the back wall. We demonstrate in subsequent sections that different phenomena are exhibited when $Fr > 2$ and when $Fr < 2$.

Finally we utilize the linearity of the governing partial differential equation (2.13) to find the solution within a domain $\mathscr{D}$ in terms of boundary integrals. We find that

$$\oint_{\partial \mathscr{D}} \boldsymbol{f} \cdot \mathrm{d}\boldsymbol{x} = 0, \tag{2.18}$$

where $f(a, b; \alpha, \beta) = -V\hat{a} + U\hat{b}$, the integration is around a curve $\partial\mathscr{D}$ in the hodograph plane such that $dx = da\hat{a} + db\hat{b}$ and

$$U = -\frac{3}{2(a-b)}tB + \frac{B}{2}\frac{\partial t}{\partial b} - \frac{t}{2}\frac{\partial B}{\partial b}, \tag{2.19}$$

$$V = \frac{3}{2(a-b)}tB + \frac{B}{2}\frac{\partial t}{\partial a} - \frac{t}{2}\frac{\partial B}{\partial a}. \tag{2.20}$$

In these expressions, $B(a, b; \alpha, \beta)$ is the Riemann function that satisfies the adjoint partial differential equation to (2.13) given by

$$\frac{\partial^2 B}{\partial a \partial b} + \frac{3}{2(a-b)}\left(\frac{\partial B}{\partial a} - \frac{\partial B}{\partial b}\right) - \frac{3B}{(a-b)^2} = 0, \tag{2.21}$$

subject to the boundary conditions that

$$\frac{\partial B}{\partial b} = -\frac{3B}{2(a-b)} \quad \text{on} \quad a = \alpha, \qquad \frac{\partial B}{\partial a} = \frac{3B}{2(a-b)} \quad \text{on} \quad b = \beta, \tag{2.22}$$

and $B(\alpha, \beta; \alpha, \beta) = 1$. In this case, the Riemann function is given by Garabedian (1986):

$$B(a, b; \alpha, \beta) = \frac{(a-b)^3}{(a-\beta)^{3/2}(\alpha-b)^{3/2}}F\left[\tfrac{3}{2}, \tfrac{3}{2}; 1; \frac{(a-\alpha)(\beta-b)}{(a-\beta)(\alpha-b)}\right], \tag{2.23}$$

where F denotes a hypergeometric function. It is possible to rewrite this hypergeometric function in terms of Legendre functions or of complete elliptic integrals of the first and second kind, and this latter form is how the function will be evaluated numerically when it is employed below.

3. Initial motion and the geometry of the characteristic plane

In this section we analyse the initial motion that results from lock-release conditions and study the implications for the form of the characteristics. In particular, we identify regions within the (x, t)-plane where both α and β take constant values, where one of α or β is constant and where both α and β vary. We term these regions 'uniform', 'simple wave' and 'complex wave', respectively. While Abbott (1961) and Rottman & Simpson (1983) have described some aspects of this structure and Ungarish (2005) has analysed the initial motion when the ambient is stratified, in this study we demonstrate how to calculate the boundaries between the regions and the solutions within them. We find that the structure and geometry of the regions depends on Fr and we show below that there are four separate cases to be considered, namely $Fr \to \infty$, $Fr = 2$, $Fr < 2$ and $Fr > 2$. In this section we treat the initial development of the flow for arbitrary value of Fr and show why there is a need to treat each of these cases separately. In subsequent sections we present the complete solutions for each value of Fr.

Initially the motion is similar to dam-break collapse centred at $x = 1$ (Whitham 1974) or, noting the analogy between the shallow water equations and those that model the one-dimensional motion of a compressible polytropic gas, the withdrawal of a piston a constant speed (Stanyukovich 1960; Garabedian 1986). When the dam is instantaneously removed there is a rarefaction wave, centred at $x = 1$ and the motion is unaffected by the finite length of the lock until the first, rearward-propagating wave has reached the rear of the lock (see figure 1). Initially $u = 0$ and $c = 1$ and so the leading rearward-propagating characteristic has value $\beta = -2$ and its path is given by $x = 1 - t$. Thus the rear wall of the lock begins to influence the motion when $t = 1$.
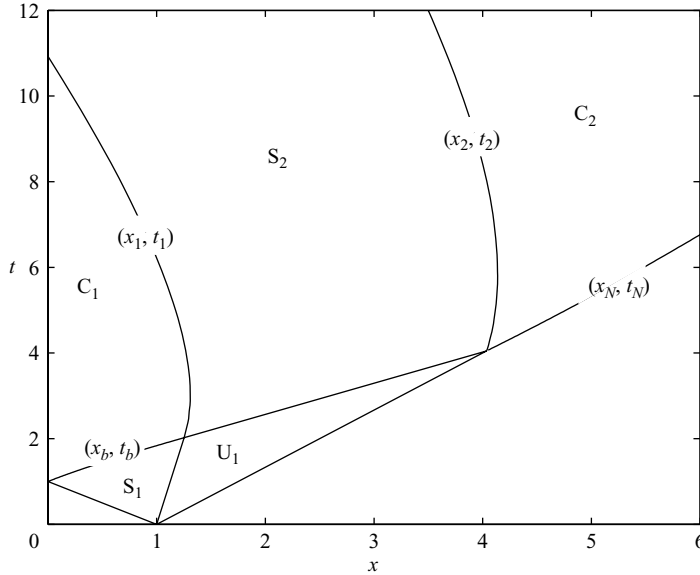
FIGURE 1. The geometry of the characteristic plane at short times after the release of the fluid from behind the lock-gate. U_1 denotes a *uniform* region within which $\alpha = 2$ and $\beta = \beta_m$; S_1 and S_2 *simple wave* regions within which $\alpha = 2$, $-2 \leqslant \beta \leqslant \beta_m$ and $\beta = \beta_m$, $|\beta_m| \geqslant \alpha \geqslant 2$, respectively; and C_1 and C_2 denote *complex wave* regions within which α and β both vary. Also plotted are characteristic curves that form boundaries between these regions. While these domains were calculated for $Fr = 1.2$, this topology is typical for all $Fr < 2$. When $Fr > 2$, the complex wave region C_1 is unbounded.

From the initial conditions, all α-characteristics have the value $\alpha = 2$ within the simple wave region S_1 (figure 1). In addition at the front of the current $u = Fr\,c$, and thus

$$u = \frac{2Fr}{Fr + 2} \qquad \text{and} \qquad c = \frac{2}{Fr + 2}. \tag{3.1}$$

This implies that the maximum value taken by the β-characteristics is $\beta = \beta_m$, where

$$\beta_m = \frac{2(Fr - 2)}{2 + Fr}, \tag{3.2}$$

and that at $x = 1$ and $t = 0$, $-2 \leqslant \beta \leqslant \beta_m$. Then we find that the β-characteristics emanating from $x = 1$ are straight lines given by

$$x = 1 + \tfrac{1}{4}(2 + 3\beta)t \tag{3.3}$$

and that within this region

$$u = \tfrac{1}{2}(2 + \beta) \qquad \text{and} \qquad c = \tfrac{1}{4}(2 - \beta). \tag{3.4}$$

It is possible to find u and c as functions of x and t by substituting for β from (3.3). The lead β-characteristic on which $\beta = \beta_m$ has equation

$$x = 1 + \frac{2(Fr - 1)}{2 + Fr}t, \tag{3.5}$$

and henceforth we will denote this characteristic by the curve (x_1, t_1). Ahead of this expansion fan there is a region within which the velocity and height fields are constant and given by (3.1). The boundary of this uniform region U_1 is the front of the motion

given by

$$x \equiv x_N(t) = 1 + \frac{2Fr}{2 + Fr}t. \tag{3.6}$$

We reiterate that the structure of the solution is such that there is a rarefaction, or expansion fan, centred on $x = 1$, with a uniform region ahead of it. The solution is given by $\alpha = 2$ and

$$\beta = \begin{cases} -2, & x < 1 - t \\ \frac{1}{3}\left(\frac{4(x-1)}{t} - 2\right), & 1 - t \leqslant x < x_1 \\ \frac{2(Fr-2)}{2+Fr}, & x_1 \leqslant x < x_N. \end{cases} \tag{3.7}$$

We note that $\beta = -2/3$ at $x = 1$ provided $Fr > 1$ (cf. Klemp, Rotunno & Skamarock 1994; Shin *et al.* 2004). This solution remains valid until the leading backward-propagating characteristic from the expansion reaches the rear boundary of the lock ($x = 0$) at $t = 1$. Thereafter the flow becomes affected by the finite lock length. There are two noteworthy features of this solution. First note that as Fr increases, the size of the domain U_1, within which there are uniform conditions, diminishes; in the limit $Fr \to \infty$, there is no longer a uniform region and the motion is always led by the characteristic on which $\alpha = \beta = 2$. Also note that the front position depends linearly on time and that the linear progression remains unaltered until a forward propagating characteristic from the rear of the lock catches up with the front.

The forward-propagating α-characteristic that forms the boundary between the regions that are and are not affected by the finite extent of the lock may be readily calculated and can be derived parametrically as $x_b(\beta)$ and $t_b(\beta)$ (see figure 1). This curve emanates from $x = 0$ at $t = 1$ and corresponds to the characteristic $\alpha = 2$. Thus along this curve we find that

$$\frac{\partial x_b}{\partial \beta} = \tfrac{1}{4}(6 + \beta)\frac{\partial t_b}{\partial \beta}, \tag{3.8}$$

while in the expansion fan region we have established (3.3). Thus we find that

$$\frac{\partial t_b}{\partial \beta} = \frac{3t_b}{4 - 2\beta}, \tag{3.9}$$

which may be integrated subject to $t = 1$ and $x = 0$ when $\beta = -2$ to yield

$$t_b = \frac{8}{(2-\beta)^{3/2}} \quad \text{and} \quad x_b = 1 + \frac{2(2+3\beta)}{(2-\beta)^{3/2}}. \tag{3.10}$$

These expressions are valid for $-2 \leqslant \beta \leqslant \beta_m$. This characteristic curve leaves the expansion fan when $\beta = \beta_m$, at a location that marks the start of the boundary with the complex wave region C_1 (see figure 1). We denote this boundary by $x_1(\alpha)$ and $t_1(\alpha)$, which is a continuation of the characteristic curve given by (3.5), now through a region in which α varies, and find that

$$t_1(2) = 8^{-1/2}(2 + Fr)^{3/2} \quad \text{and} \quad x_1(2) = 1 + 2^{-1/2}(Fr - 1)(2 + Fr)^{1/2}. \tag{3.11}$$

We observe that, as indicated above, in the limit $Fr \to \infty$, $t_1(2), x_1(2) \to \infty$. Thus in this limit the characteristic from the rear of the lock does not intersect the front.

Subsequent characteristics emanating from $x = 0$ have values of α less than 2 and are no longer propagating through a simple expansion fan solution. To calculate the
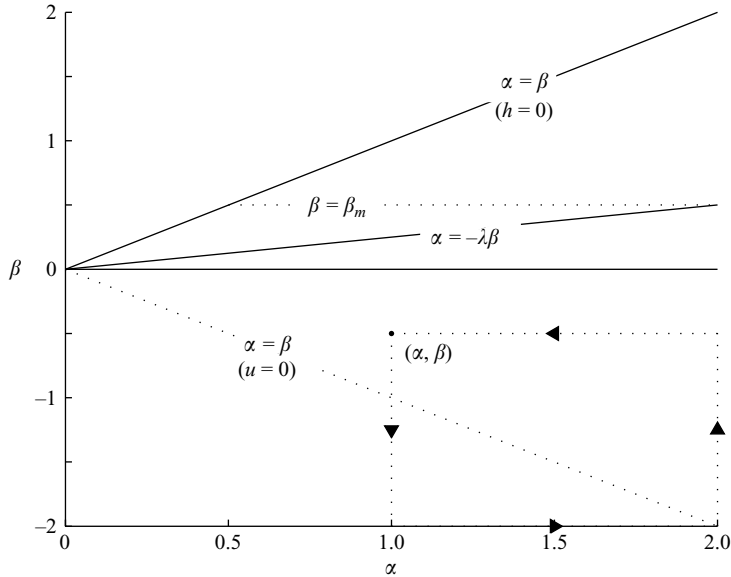
FIGURE 2. The hodograph plane: the dynamic Froude number condition holds along the line $\alpha = -\lambda\beta$, while the complex wave region C_1 corresponds to $|\beta_m| \leqslant \alpha \leqslant 2$ and $-2 \leqslant \beta \leqslant \beta_m$. Integration along the line segments (------) permits the solution to be derived within C_1. In this sketch $Fr > 2$.

solution in this region we employ the hodograph variables and integrate around a rectangular boundary in the (α, β)-plane with vertices at $(2, -2)$, $(2, \beta)$, (α, β) and $(\alpha, -2)$, as illustrated in figure 2. For this domain (2.18) becomes

$$0 = \int_{-2}^{\beta} U(2, b; \alpha, \beta)\, \mathrm{d}b - \int_2^{\alpha} V(a, \beta; \alpha, \beta)\, \mathrm{d}a + \int_{\beta}^{-2} U(\alpha, b; \alpha, \beta)\, \mathrm{d}b$$

$$- \int_{\alpha}^2 V(a, -2; \alpha, \beta)\, \mathrm{d}a. \tag{3.12}$$

Integration by parts and using the conditions along characteristics and the boundary conditions for the Riemann function yields

$$t = B(2, -2; \alpha, \beta). \tag{3.13}$$

This expression is valid within a region that is bounded by the $\alpha = 2$ characteristic emanating from $x = 0$, (x_b, t_b), for which $-2 \leqslant \beta \leqslant \beta_m$, and by a $\beta = \beta_m$ characteristic that starts from $t = t_1(2)$ and $x = x_1(2)$. Integrating along the latter characteristic on which $t \equiv t_1(\alpha) = t(\alpha, \beta_m)$, we find that

$$x_1(\alpha) = x_1(2) + \int_2^{\alpha} \tfrac{1}{4}(\alpha + 3\beta_m)\frac{\partial t_1}{\partial \alpha}\, \mathrm{d}\alpha. \tag{3.14}$$

Thus given $x_1(\alpha)$ and $t_1(\alpha)$, we may deduce the geometry of the domain C_1 within the (x, t)-plane (see figure 1). In particular, we note that

$$x_1(-\beta_m) = 0 \qquad \text{provided} \qquad Fr < 2, \tag{3.15}$$

but if $Fr \geqslant 2$, then $x_1, t_1 \to \infty$ as $\alpha \to \beta_m$ (see the Appendix). Thus when $Fr < 2$ the complex wave region, C_1, is bounded as shown in figure 1, whereas for $Fr \geqslant 2$ it is unbounded.

We may also calculate the trajectory of x_b, t_b in the uniform region ahead of the expansion fan to find the position where this characteristic intersects the front of the flow. From this point there is another β-characteristic on which $\beta = \beta_m$, which we denote by $x_2(\alpha)$ and $t_2(\alpha)$, with the intersection with the front occurring when $\alpha = 2$ (figure 1). For $t > t_1(2)$, the $\alpha = 2$ characteristic is given by

$$x_b - x_1(2) = \tfrac{1}{4}(6 + \beta_m)(t_b - t_1(2)), \tag{3.16}$$

and so this intersects the front at

$$t_2(2) = 2^{-1/2}(Fr + 2)^{3/2} \qquad \text{and} \qquad x_2(2) = 1 + 2^{1/2}Fr(Fr + 2)^{1/2}. \tag{3.17}$$

This is the first time at which the front of the current is affected by the finite extent of the lock from which it was released. It may be interpreted as the end of the slumping phase, defined by Rottman & Simpson (1983) and it marks the end of the period during which the front of the current moves with a constant speed. The $\beta = \beta_m$ characteristic generated from this point satisfies

$$\frac{\partial x_2}{\partial \alpha} = \tfrac{1}{4}(\alpha + 3\beta_m)\frac{\partial t_2}{\partial \alpha}, \tag{3.18}$$

and α-characteristics arriving at this location satisfy

$$x_2 = x_1 + \tfrac{1}{4}(3\alpha + \beta_m)(t_2 - t_1). \tag{3.19}$$

Hence substituting for x_2 and integrating, we find that

$$t_2(\alpha) = t_1(\alpha) + \frac{8}{(\alpha - \beta_m)^{3/2}} \qquad \text{and} \qquad x_2(\alpha) = x_1(\alpha) + \frac{2(3\alpha + \beta_m)}{(\alpha - \beta_m)^{3/2}}. \tag{3.20}$$

4. Complete solutions for the flow

In §3 we constructed the characteristics at relatively short times after the release of the fluid from behind the lock gate, showing that there were domains in which the flow was uniform in addition to simple wave and complex wave regions. The complete flow solutions may be readily calculated, although, as will be demonstrated below, the nature of the solutions depends upon the magnitude of Fr. Thus we analyse separate cases in the following subsections, first dealing with the special cases $Fr \to \infty$ (§4.1) and $Fr = 2$ (§4.2), before analysing the somewhat more complicated regimes $Fr < 2$ (§4.3) and $Fr > 2$ (§4.4).

4.1. $Fr \to \infty$

In the limit $Fr \to \infty$, the structure of the characteristics in the (x, t)-plane is considerably simplified and it is possible to derive the analytical solution for the bounded dam-break flow in terms of known functions. There is no uniform region ahead of the expansion fan centred on $x = 1$ and the $\alpha = 2$ characteristic from the rear wall, $x_b(t)$, never catches the front, $x_N = 2t + 1$. Thus we may readily evaluate the entire solution: for $t < 1$ and $1 - t < x < x_N$ and for $t > 1$ and $x_b < x < x_N$, we find that

$$\alpha = 2 \qquad \text{and} \qquad \beta = \frac{1}{3}\left(\frac{4(x - 1)}{t} - 2\right). \tag{4.1}$$

For $t > 1$ and $0 < x < x_b$

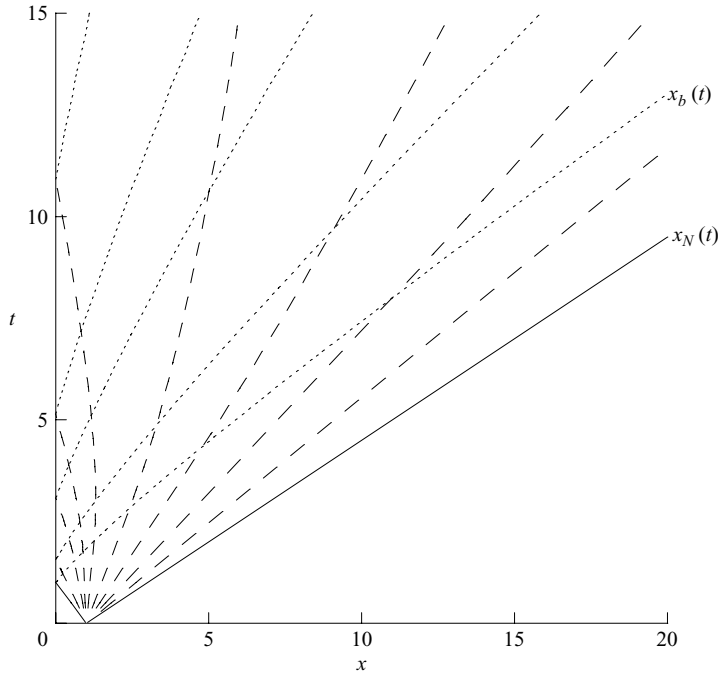$$t = B(2, -2; \alpha, \beta), \qquad \alpha + \beta > 0. \tag{4.2}$$

FIGURE 3. The characteristic curves when $Fr \to \infty$, showing the α-characteristics (······)
for $\alpha = 0, 0.5, 0.75, 1.0, 1.5, 2.0$ and the β-characteristics (– – –) for $\beta = -2.0, -1.5, -1.0,$
$-0.75, -0.5, 0, 0.5, 0.75, 1.0, 1.5, 2.0$. Also plotted are the front, $x_N(t)$ and the boundary
between the complex and simple wave regions, $x_b(t)$.

We plot the characteristic curves in the (x, t)-plane in figure 3, while profiles of $u(x, t)$
and $h(x, t)$ are plotted in figure 4. Note that the height and velocity fields remain
continuous but that their gradients are discontinuous at $x = x_b(t)$. This point marks
the foremost location at which the flow is affected by the presence of the rear wall
of the lock.

4.2. $Fr = 2$

When $Fr = 2$ the front corresponds to $\beta = 0$ and thus we find a rather different
configuration of characteristics in the (x, t)-plane: the front occurs within a simple
wave region, S_2 and there is no complex wave region C_2. Furthermore, as discussed
above and demonstrated in the Appendix, the complex wave region, C_1, becomes
unbounded when $Fr = 2$.

The lead $\alpha = 2$ characteristic intersects the front at $(x_2(2), t_2(2))$. Thereafter the
motion of the front is no longer linearly dependent on time, but rather is determined
from (2.16) and given by

$$\frac{\partial x_N}{\partial \alpha} = \tfrac{1}{2}\alpha \frac{\partial t_N}{\partial \alpha}, \qquad (4.3)$$

while α-characteristics in the simple wave region S_2 have $\beta = 0$ and are given by

$$x = x_1(\alpha) + \tfrac{3}{4}\alpha \left[t - t_1(\alpha)\right]. \qquad (4.4)$$

Thus we find that

$$t_N(\alpha) = 2t_1(\alpha) - \frac{1}{\alpha^3} \int_2^\alpha 3a^2 t_1 \, \mathrm{d}a \qquad (4.5)$$
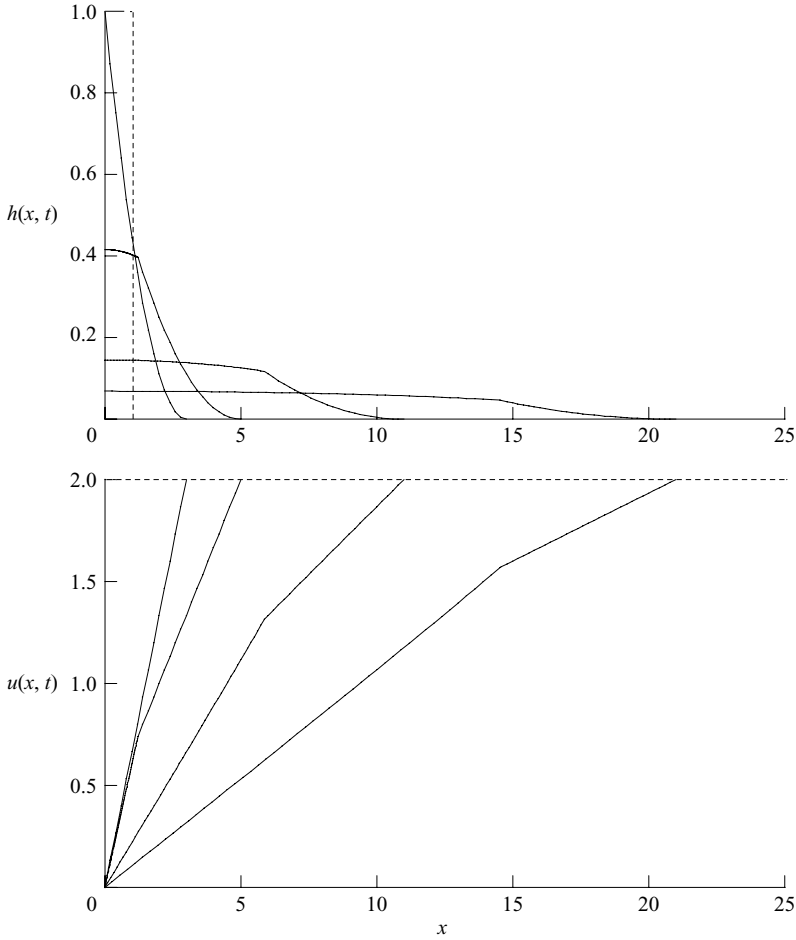
FIGURE 4. The height, $h(x, t)$, and velocity, $u(x, t)$, fields as functions of distance from the rear lock wall, x, at $t = 1, 2, 5, 10$ when $Fr \to \infty$. Also plotted as dashed lines are the initial lock-release condition for h and the maximum velocity at the front, $u = 2$.

and

$$x_N(\alpha) = 1 + \tfrac{3}{4}\alpha t_N(\alpha) - \tfrac{1}{2}\alpha t_1(\alpha) - \tfrac{1}{4} \int_2^\alpha t_1 \, \mathrm{d}a. \tag{4.6}$$

We plot the characteristic curves in figure 5 and some velocity and height profiles in figure 6. Note that at $t = 5$ parts of these profiles orginate from the complex wave region, C_1, the simple wave region, S_2 and the uniform region, U_1.

4.3. $Fr < 2$

When $Fr < 2$, we have demonstrated that the complex wave region C_1 is bounded by the characteristic curve (x_1, t_1) on which $\beta = \beta_m$. Specifically we have shown that

$$x_1(-\beta_m) = 0 \quad \text{and} \quad t_1(-\beta_m) = B(2, -2; -\beta_m, \beta_m) \equiv \left(\frac{8}{-\beta_m^3}\right)^{1/2} P_{1/2}\left(\frac{-4 - \beta_m^2}{4\beta_m}\right),$$
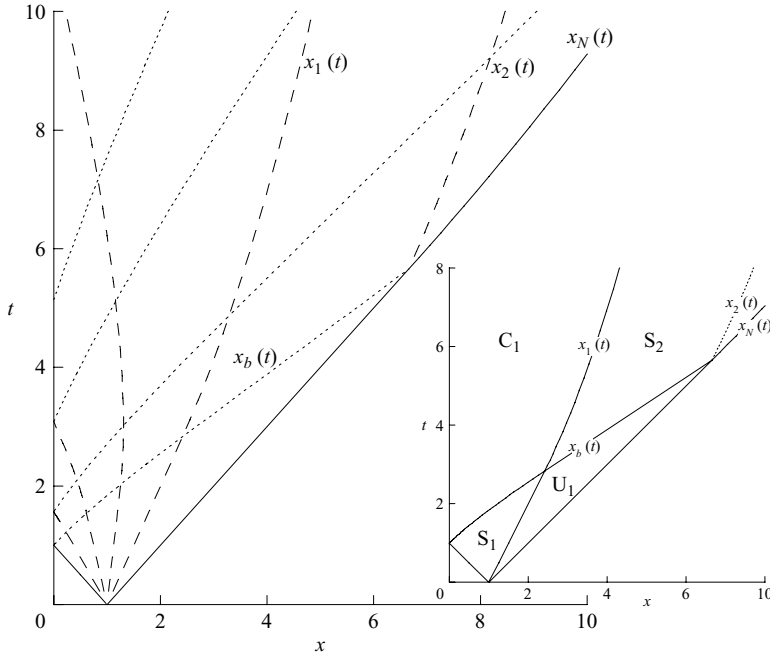
$$\tag{4.7}$$

FIGURE 5. The characteristic curves when $Fr = 2$, showing the α-characteristics ($\cdots$) for $\alpha = 0.75, 1.0, 1.5, 2.0$ and the β-characteristics ($---$) for $\beta = -2.0, -1.5, -1.0, -0.5$. Also plotted are the front, $x_N(t)$, the boundary between the complex and simple wave regions C_1 and S_1, $x_b(t)$ and the β-characteristics, $x_1(t)$ and $x_2(t)$ that bound the complex wave regions C_1 and emerge from the intersection of $x_b(t)$ and $x_N(t)$, respectively. The inset sketch depicts the uniform, simple wave and complex wave regions.

where $P_{1/2}$ is a Legendre function of order $\frac{1}{2}$. Importantly, recall that when $Fr < 2$, $\beta_m < 0$ and so these expressions are real-valued. A forward-propagating α-characteristic emanates from this point, on which $\alpha = -\beta_m$, and we denote this curve by (x_3, t_3) (figure 7). Through the simple wave region S_2 it is given by

$$x_3 = -\tfrac{1}{2}\beta_m(t - t_1(-\beta_m)). \tag{4.8}$$

It intersects with $\beta = \beta_m$ characteristic, (x_2, t_2), to form a boundary of the complex region C_2, which is analysed below. The $\beta = \beta_m$ characteristic continues beyond this intersection to form a boundary of a region within which $\beta = \beta_m$ and $\alpha = -\beta_m$. We denote this uniform region by U_2 and find that the characteristic reaches $x_2 = 0$ at $t_2 = t_1(-\beta_m) + 16(-2\beta_m)^{3/2}$. This is the first time at which characteristic data have propagated from the back wall, been reflected at the front and then returned to the back wall. This pattern of wave-like disturbances propagating along the entire length of the current and reflected between the back wall and the moving front will be continued throughout the subsequent motion. Indeed by considering the path of this disturbance in the hodograph plane, it is straightforward to see that the forward-propagating characteristics have value $\alpha = 2\lambda^{n-1}$, while the backward-propagating characteristics have value $\beta = -2\lambda^n$ for the nth reflection (figure 8). It is also noteworthy that within U_2 the velocity vanishes.

Beyond the uniform region, U_2, there is a simple wave region, S_3, which is bounded by an $\alpha = -\beta_m$ characteristic. We denote this characteristic curve by (x_4, t_4) and
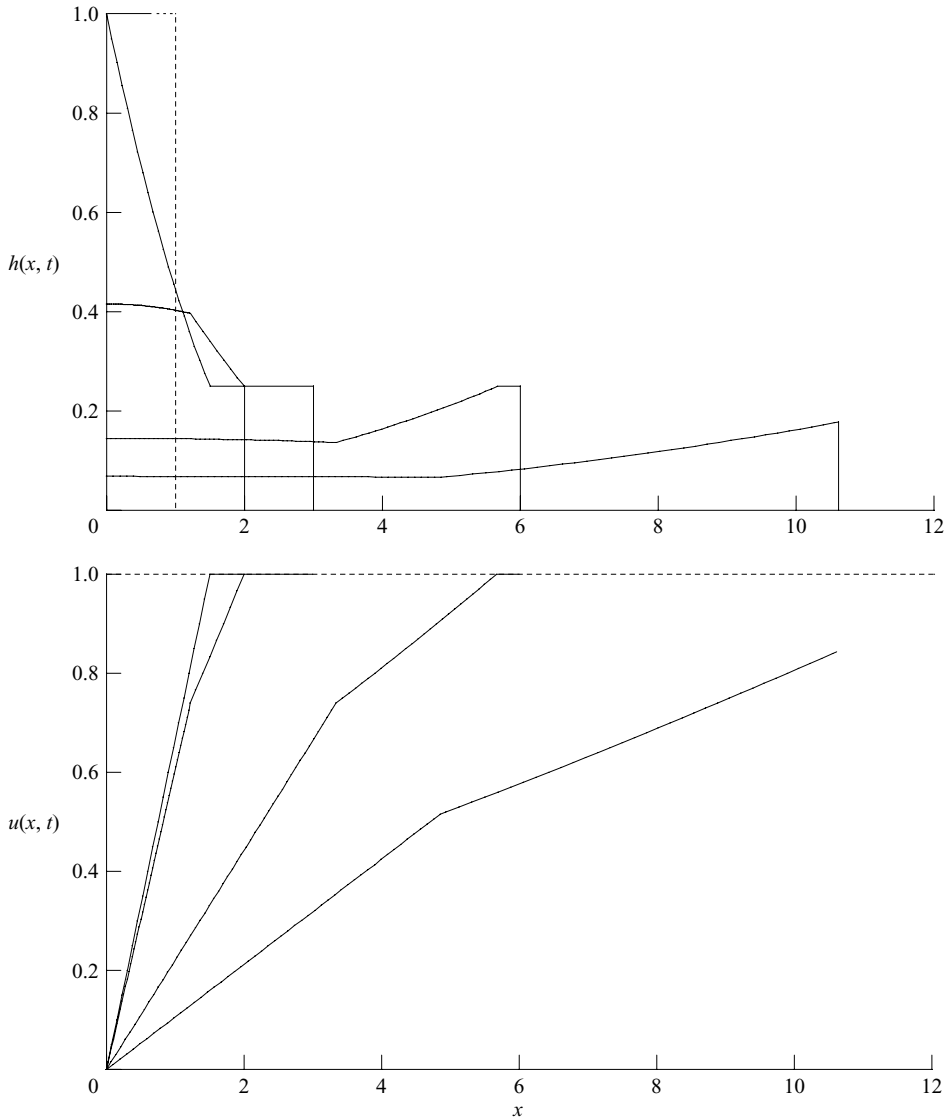
FIGURE 6. The height, $h(x, t)$, and velocity, $u(x, t)$, fields as functions of distance from the rear lock wall, x, at $t = 1, 2, 5, 10$ when $Fr = 2$. Also plotted as dashed lines are the initial lock-release condition for h and the maximum velocity at the front, $u = 1$.

find that

$$t_4(\beta) = t_3(\beta) + \frac{8}{(-\beta_m - \beta)^{3/2}} \qquad \text{and} \qquad x_4(\beta) = x_3(\beta) + \frac{2(-\beta_m + 3\beta)}{(-\beta_m - \beta)^{3/2}}, \qquad (4.9)$$

where $t_3(\beta)$ and $x_3(\beta)$ are the characteristic curve that bounds the complex wave region C_2 (see figure 7).

We now construct the solution within the complex wave region C_2. In general the solution at a point (α, β) is given by the following boundary integrals in the
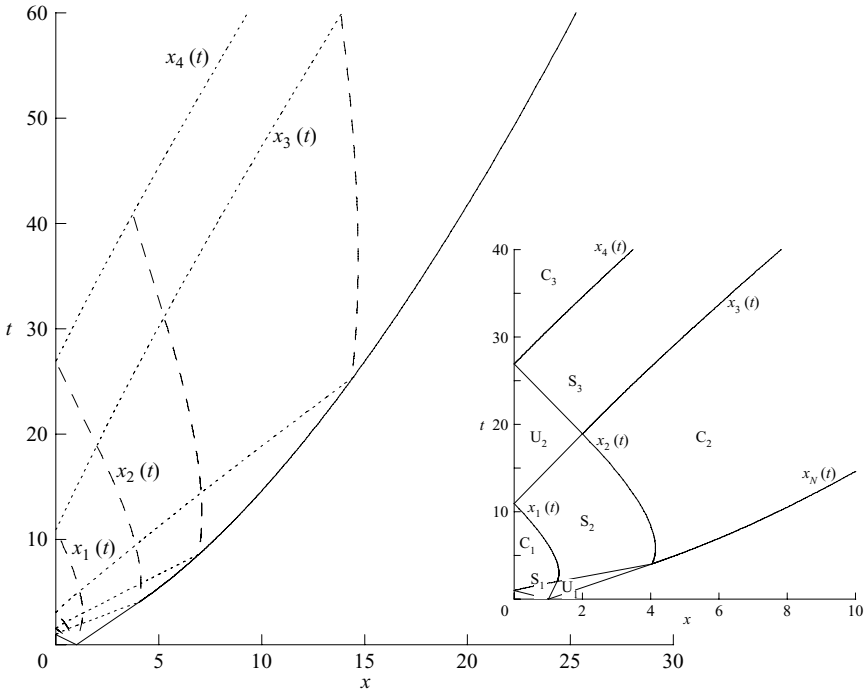
FIGURE 7. The characteristic curves when $Fr = 1.2$, showing the α-characteristics ($\cdots\cdots$) for $\alpha = 1.0, 1.5, 2.0$ and the β-characteristics ($- - -$) for $\beta = -2.0, -1.5, -1.0, -0.375, -0.25$. Also plotted are the front, $x_N(t)$, the $\beta = -0.5$ characteristics, $x_1(t)$ and $x_2(t)$ that bound the complex wave regions C_1 and C_2, respectively and the $\alpha = 0.5$ characteristics $x_3(t)$ and $x_4(t)$ that bound the complex wave regions C_2 and C_3, respectively. The inset sketch depicts the uniform, simple wave and complex wave regions.
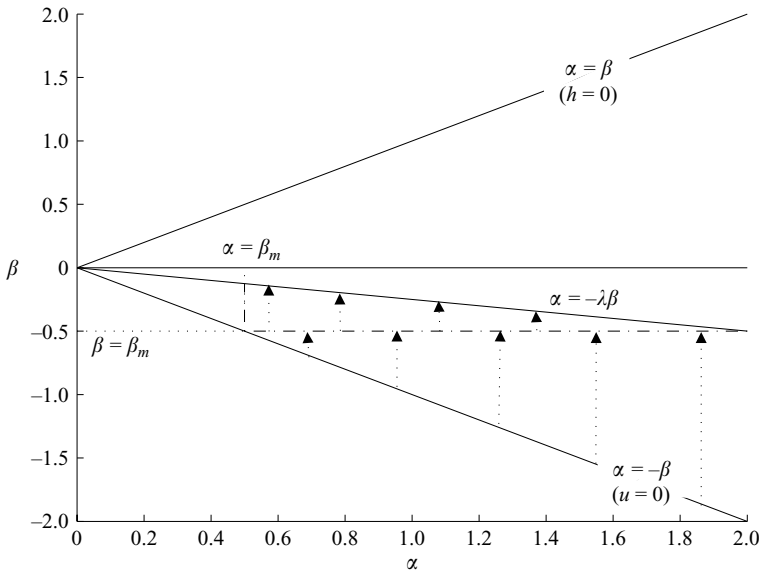

FIGURE 8. The hodograph plane for $Fr = 1.2$. Complex wave region C_1 is bounded by the characteristic $\beta = \beta_m$, while complex wave region C_2 lies in the region $\{(\alpha, \beta) : \alpha > -\beta_m ; \beta > \beta_m ; \alpha + \lambda\beta \leqslant 0\}$. Within both of these regions, evolution along α-characteristics is the direction of increasing β, as indicated by the arrows.

hodograph plane (figure 8):

$$
0 = -\int_2^\alpha V(a, \beta_m; \alpha, \beta)\, \mathrm{d}a + \int_{\beta_m}^\beta U(\alpha, b; \alpha, \beta)\, \mathrm{d}b - \int_\alpha^{-\beta/\lambda} V(a, \beta; \alpha, \beta)\, \mathrm{d}a
$$

$$
+ \int_{-\beta/\lambda}^2 (-V(a, \lambda a; \alpha, \beta) - \lambda U(a, \lambda a; \alpha, \beta))\, \mathrm{d}a. \quad (4.10)
$$

This expression may be integrated by parts to yield

$$
t(\alpha, \beta) = \tfrac{1}{2} B(-\beta/\lambda, \beta; \alpha, \beta) t(-\beta/\lambda, \beta) + \tfrac{1}{2} B(2, \beta_m; \alpha, \beta) t_2(2)
$$

$$
+ \int_2^\alpha \left(\frac{\partial t_2}{\partial a} + \frac{3 t_2}{2(a - \beta_m)} \right) B(a, \beta_m; \alpha, \beta)\, \mathrm{d}a
$$

$$
+ \int_{-\beta/\lambda}^2 \tfrac{1}{2} t(a, -\lambda a) \left(\frac{3 Fr B(a, -\lambda a; \alpha, \beta)}{2a} - \frac{\partial B}{\partial a} - \lambda \frac{\partial B}{\partial b} \right) \mathrm{d}a. \quad (4.11)
$$

However we have not yet computed the values of $t(\alpha, -\lambda\alpha)$, which are needed for the evaluation of the last integral in (4.11). This corresponds to the times, t_N, along the front. Thus we must solve an initial problem to calculate t along the front ($\beta = -\lambda\alpha$). We substitute $\beta = -\lambda\alpha$ in (4.10) and using the boundary condition (2.17), deduce the following integral equation for $t(\alpha, -\lambda\alpha)$:

$$
t(\alpha, -\lambda\alpha) = B(2, \beta_m; \alpha, -\lambda\alpha) t_2(2) + 2 \int_2^\alpha B(a, \beta_m; \alpha, -\lambda\alpha) \left(\frac{\partial t_2}{\partial a} + \frac{3 t_2}{2(a - \beta_m)} \right) \mathrm{d}a
$$

$$
+ \int_\alpha^2 \frac{3 Fr B t}{2a} - t \left(\frac{\partial B}{\partial a} + \lambda \frac{\partial B}{\partial b} \right) \mathrm{d}a. \quad (4.12)
$$

This is an inhomogeneous Volterra equation of the second kind, which may be solved numerically by iteration (Arfken & Weber 1995). Typically we achieved a converged solution after 10 iterations. Next, having calculated $t(\alpha, -\lambda\alpha)$, we may use (4.11) to find the solution throughout the whole domain. The values of x may also be readily calculated. Given that $x_2(\alpha)$ specifies x along the characteristics $\beta = \beta_m$, it is then possible to integrate forward along α-characteristics in the region C_2. We note that $t(\alpha, \beta)$ and $x(\alpha, \beta)$ are continuous across the boundary between S_2 and C_2, but that their normal derivatives may not be continuous across this boundary.

We plot profiles of the velocity and height fields in figure 9. We note that the profile at $t = 20$ contains contributions from the uniform region U_2, the simple wave region S_3 and the complex wave region C_2. At this time, and at other times when there are contributions from the uniform region U_2, the velocity vanishes close to the source because $\alpha + \beta = 0$.

4.4. *Fr > 2*

When $Fr > 2$ we have shown that $x_1, t_1 \to \infty$ as $\alpha \to -\beta_m$ and thus the complex wave region, C_1, and the simple wave region, S_2 are unbounded (see figures 1 and 10). The complex wave region that includes the front, C_2, is bounded on one side by the characteristic $x_2(\alpha)$ and $t_2(\alpha)$ on which $\beta = \beta_m$. Subsequent β-characteristics emerge from the front and since at the front $\alpha = -\lambda\beta$ and $\lambda < 0$, as α decreases, so does β. Thus in the hodograph plane, the direction of propagation along lines of constant α in this region has reversed (figure 11). Equivalently, the Jacobian changes sign at $\beta = \beta_m$ and so the hodograph plane develops a fold and the complex wave region C_2 lies in the domain $\{(\alpha, \beta) : \beta < \beta_m; \alpha - \beta > 0; \beta + \lambda\alpha > 0\}$.
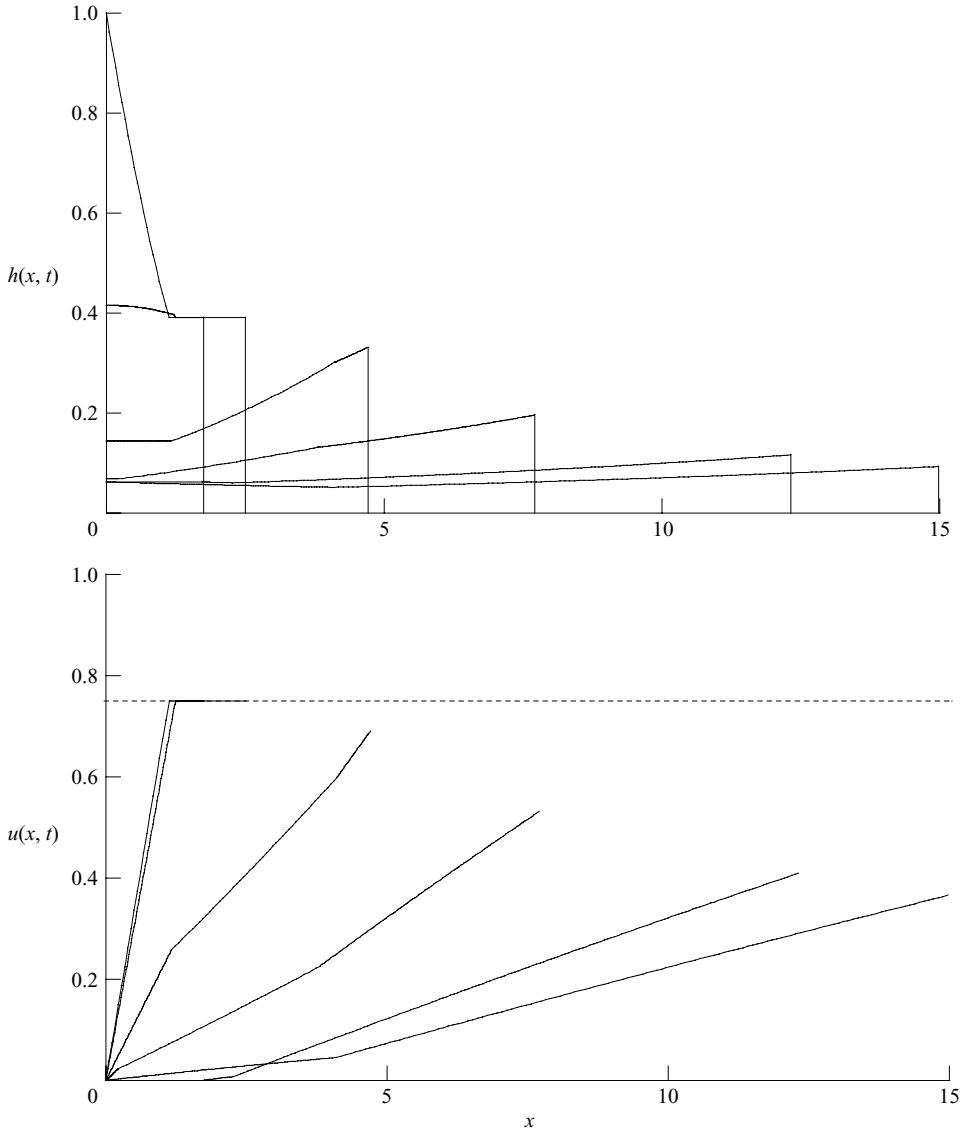
FIGURE 9. The height, $h(x, t)$, and velocity, $u(x, t)$, fields as functions of distance from the rear lock wall, x, at $t = 1, 2, 5, 10, 20, 26.92$ when $Fr = 1.2$. Also plotted is the maximum velocity at the front, $u = 3/4$ (- - - -). Note that at $t = 1$ and $t = 2$, the current attains the same velocity and height throughout a region at the front (rendering the velocity profiles hard to distinguish in this plot). Note also that at $t = 20$, u and $\partial h/\partial x$ vanish in a region close to the rear of the lock.

The solution given by (4.11) and (4.12) is valid provided the hodograph transformation remains invertible, which is equivalent to demanding that the Jacobian remains finite, but non-zero. When $Fr > 2$, we find that this condition is not held; specifically we find that the Jacobian vanishes within C_2 at a point $(\alpha, \beta) = (\alpha^*, \beta_m)$, where $\partial t/\partial \beta = 0$. This implies that at this point the β-characteristics, emanating from the front, intersect. Thus it is no longer possible to construct the solution from the
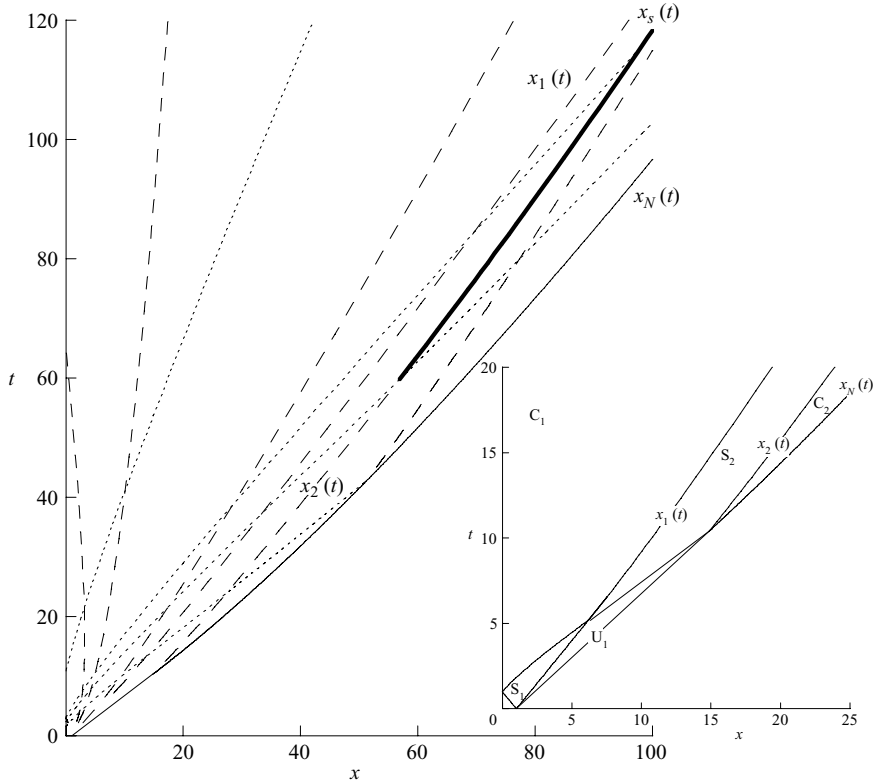
FIGURE 10. The characteristic curves when $Fr = 4$, showing the α-characteristics ($\cdots\cdots$) for $\alpha = 0.5, 1.0, 1.1677, 1.5$ and the β-characteristics ($---$) for $\beta = -0.2, 0, 0.5$. Also plotted are the front, $x_N(t)$, the $\beta = 0.667$ characteristics, $x_1(t)$ and $x_2(t)$ that bound the complex wave regions C_1 and C_2 and the shock, $x_s(t)$ (———) , across which α and β are discontinuous. The inset depicts the wave regions.

two integral equations, (4.11) and (4.12); rather the solution includes a discontinuity (shock) as is elucidated below.

We may evaluate $\partial t / \partial \beta$ at $\beta = \beta_m$ from (4.11) and when $Fr = 4$, to find that

$$\left(\frac{\partial t}{\partial \beta}\right)_{\beta=2/3} = 0 = -\frac{54\sqrt{3}(15\alpha - 16)}{(3\alpha - 2)^{3/2}} + \int_2^\alpha \left(\frac{\partial t_1}{\partial \alpha} + \frac{3t_1}{2(a - 2/3)}\right)\frac{\partial B}{\partial \beta}\left(a, \tfrac{2}{3}; \alpha, \tfrac{2}{3}\right) da.$$

(4.13)

Thence we find that $\partial t / \partial \beta = 0$ at $\alpha \equiv \alpha^* = 1.168$, for which $t = 59.78$.

The solution determined by the integration of (4.11) and (4.12) is valid in the region $\{(\alpha, \beta) : \beta < \beta_m; \alpha > \alpha_*; \beta + \lambda\alpha > 0\}$. For $\alpha < \alpha_*$, there is a tear in the hodograph plane and the solutions jump discontinuously from the simple wave region S_2 within which $\beta = \beta_m$ to the curve given by (α_s, β_s) as illustrated in figure 11. We now demonstrate how to calculate this curve in the hodograph plane and thus elucidate the height and velocity profiles that contain discontinuities.

In terms of the original dependent variables of the shallow water equations, if there is a discontinuity at position $x_s(t)$, moving with speed $s = dx_s/dt$, then across the
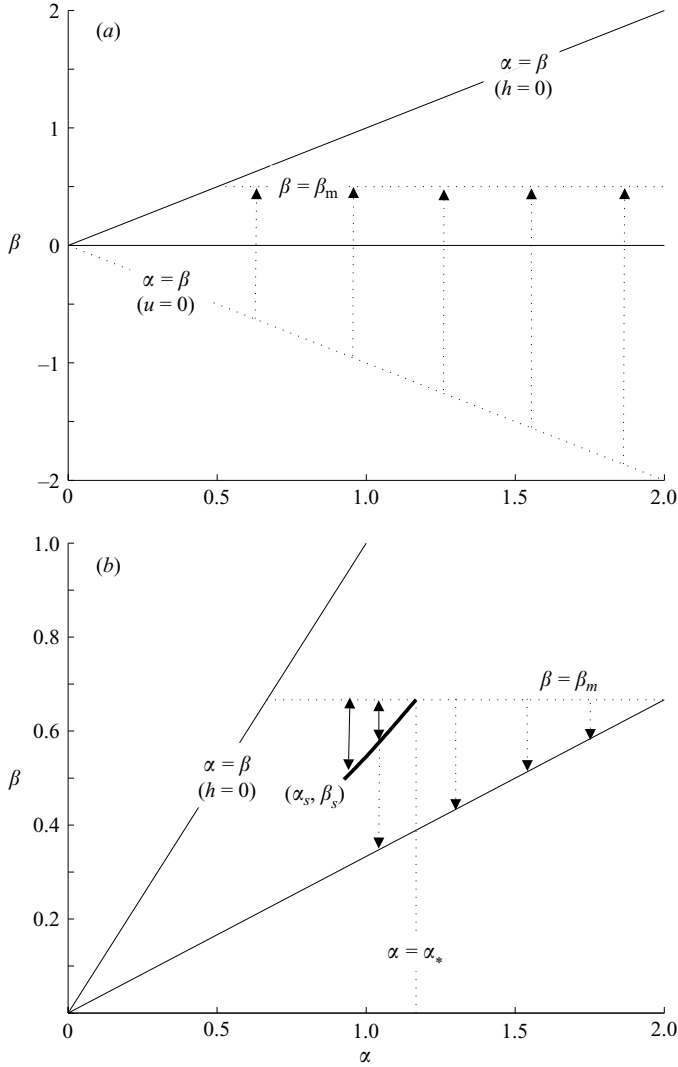
FIGURE 11. The hodograph plane for $Fr = 4$. Complex wave region C_1 is bounded by the characteristic $\beta = \beta_m$ and within it the motion evolves so that the magnitude of β increases along α-characteristics, as indicated by the arrows in (*a*). Within complex wave region C_2, the hodograph develops a fold and the motion now evolves so that β decreases along α-characteristics, as indicated by the arrows in (*b*). At $(\alpha, \beta) = (\alpha_*, \beta_m)$ the hodograph transformation becomes non-invertible. Thereafter a shock develops and the hodograph plane develops a 'tear', as α and β jump discontinuously to α_s and β_s.

discontinuity the following dimensionless conditions hold:

$$[(u - s)h]_{x_s^-}^{x_s^+} = 0 \quad \text{and} \quad [(u - s)^2 h + \tfrac{1}{2}h^2]_{x_s^-}^{x_s^+} = 0, \qquad (4.14)$$

where x_s^+ and x_s^- denote the values of the variables ahead of and behind the discontinuity, respectively. These conditions represent the conservation of mass and momentum fluxes across the discontinuity. Therefore it is possible to relate the hodograph variables ahead of the shock, α_s, β_s, to those behind the shock, α, β_m, and the shock speed, s. Although the independent variables of the hodograph plane jump

discontinuously, both t and x are continuous, denoted by t_s and x_s, respectively, and this continuity will be used to construct the solution.

In the region $t \leqslant t_s$ the characteristics reaching the shock initially emerge from the simple wave region S_2 within which $\beta = \beta_m$. Hence we may parameterize the shock speed and shock curve as functions of α. The characteristics reaching the shock are given by

$$x_s = x_1(\alpha) + \tfrac{1}{4}(3\alpha + \beta_m)(t_s - t_1(\alpha)), \tag{4.15}$$

while the position of the shock moves according to

$$\frac{\mathrm{d}x_s}{\mathrm{d}\alpha} = s \frac{\mathrm{d}t_s}{\mathrm{d}\alpha}. \tag{4.16}$$

Hence eliminating x_s between (4.15) and (4.16) yields

$$t_s = \frac{1}{F(\alpha)} \left[\int_{\alpha_*}^{\alpha} \left(\tfrac{1}{2}(\alpha' - \beta_m)\frac{\partial t_1}{\partial \alpha'} + \tfrac{3}{4}t_1 \right) \frac{F(\alpha')}{\tfrac{1}{4}(3\alpha' + \beta_m) - s} \, \mathrm{d}\alpha' + t(\alpha_*) \right], \tag{4.17}$$

where

$$F(\alpha) = \exp\left(-\int_{\alpha_*}^{\alpha} \frac{3}{3\alpha' + \beta_m - 4s} \, \mathrm{d}\alpha' \right). \tag{4.18}$$

This expression implies that t_s is determined as a function of the unknown shock speed s.

When $t > t_s$, we may calculate the solution by evaluating the boundary integrals in (2.18) along the curve $\{C_1 \cup C_2 \cup C_3 \cup C_4\}$ in the hodograph plane, where C_1 is the portion of the shock curve (α_s, β_s), C_2 is the line segment from (α_s, β_s) to (α_s, β), C_3 is the line segment from (α_s, β) to (α_*, β), and C_4 is the line segment from (α_*, β) to (α_*, β_m). Integrating by parts, we thus derive

$$t(\alpha_s, \beta) = B(\alpha_*, \beta_m; \alpha_s, \beta)t(\alpha_*, \beta_m) + \int_{\beta}^{\beta_m} \left(\frac{3t(\alpha_*, b)}{2(\alpha_* - b)} - \frac{\partial t}{\partial b} \right) B(\alpha_*, b; \alpha_s, \beta) \, \mathrm{d}b$$

$$+ \int_{\alpha_*}^{\alpha} B(a_s, b_s; \alpha_s, \beta) \left[\frac{3t(a_s, b_s)}{2(a_s - b_a)} + \frac{\partial t}{\partial a}\frac{\mathrm{d}a_s}{\mathrm{d}\alpha} \right] + t(a_s, b_s)\frac{\partial B}{\partial b}\frac{\mathrm{d}b_s}{\mathrm{d}\alpha} \, \mathrm{d}\alpha, \tag{4.19}$$

where $a_s = \alpha_a(\alpha)$ and $b_s = \beta_s(\alpha)$. In this expression we may set $\beta = \beta_s$ and this yields a second expression for t_s. Since t_s must be continuous across the shock we may solve (4.17) and (4.19) simultaneously to deduce the shock speed s as a function of the upstream characteristic variable α. In fact in our numerical computation of t_s from (4.19), we find it convenient to substitute for $\partial t_s / \partial a$ from (4.17) and then to solve the integral equation numerically by iteration.

Having found t_s along the shock trajectory, it is then straightforward to calculate t at interior points using (4.19). The position of the shock curve, x_s, may be calculated directly from (4.15) and $x(\alpha, \beta)$ may be computed by integrating along α-characteristics. This completes the solution ahead of the shock. This method is valid until the shock curve, which is moving forward less rapidly than the characteristics on which $\beta = \beta_m$, enters the complex wave region C_1. Thereafter the conditions upstream of the shock are determined from more complex expressions.

We plot the trajectory of the shock curve (α_s, β_s) in figure 11, showing how it deviates from $\beta = \beta_m$ and creates a tear in the hodograph plane. In figure 10 we plot the characteristics and shock trajectory in the (x, t)-plane. The $\alpha = 1.1677$ characteristic is the α-characteristic with the largest value of α that does not encounter the shock. Finally we plot some snapshots of the height and velocity profiles (figure 12), noting
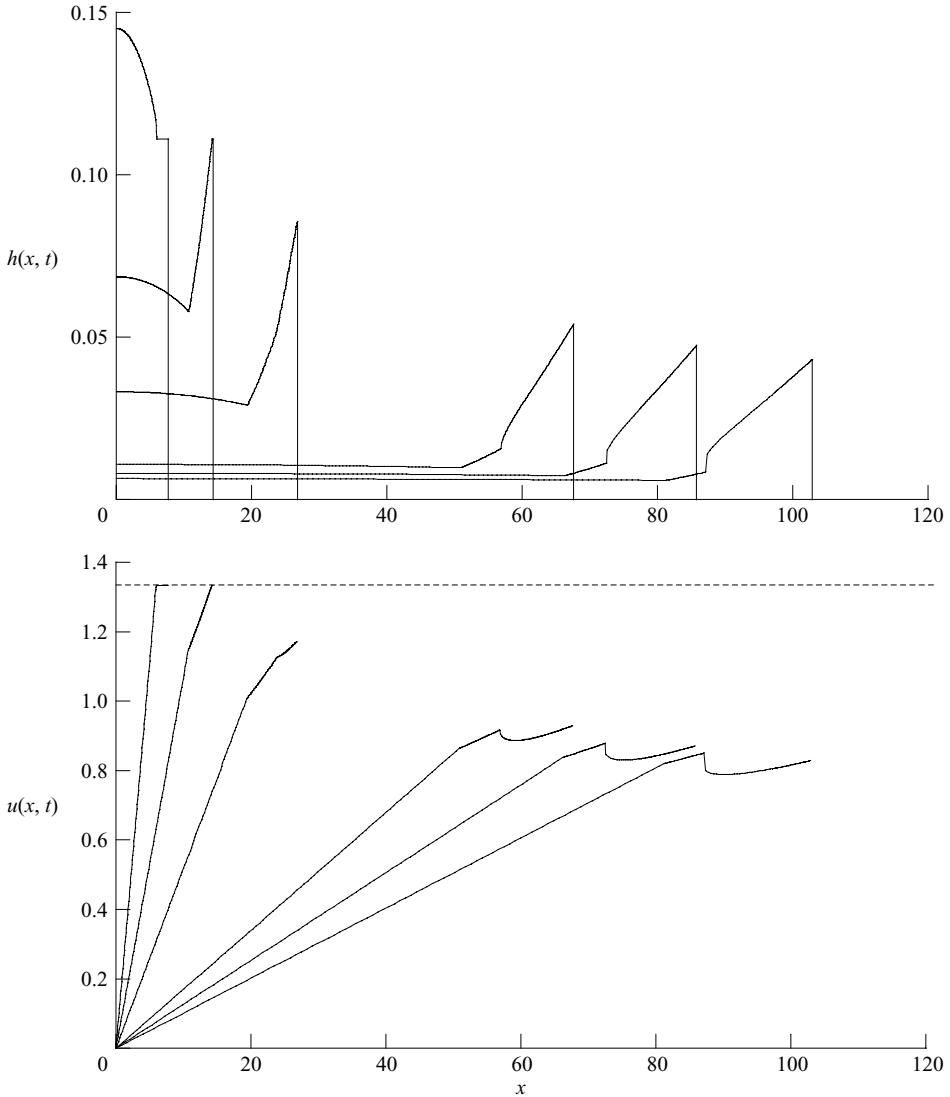
FIGURE 12. The height, $h(x, t)$, and velocity, $u(x, t)$, fields as functions of distance from the rear lock wall, x, at $t = 5, 10, 20, 59.78, 80, 100$ when $Fr = 4$. Also plotted is the maximum velocity at the front, $u = 4/3$ (- - - -) .

that the discontinuity emerges at a relatively late time, $t = 59.78$, and that its magnitude grows in time.

5. Summary and conclusion

We have modelled the motion of gravity currents and dam-break flows using shallow water equations and have demonstrated how to calculate the motion that results from the release of initially stationary fluid from behind a rapidly removed lock gate. Such lock-release conditions have been important initial configurations in both experimental and theoretical investigations of these flows. The key novel contribution of this study is that we have developed solutions using analytical

techniques, supplemented by simple numerical evaluations and quadrature, rather than directly integrating the governing partial differential equations numerically. This is possible by a transformation to hodograph variables, which linearizes the governing equations. This approach offers many advantages. First it provides new insight into these flows and indicates very clearly the different phenomena that arise for different values of the Froude number at the front. However, it also provides a series of accurate solutions against which results from the numerical integration of the shallow water equations may be tested. This is valuable because the solutions feature moving fronts and positions where the dependent variables, or their derivatives, are discontinuous and both of these features pose some difficulties for many numerical schemes.

The results build upon and significantly extend previous analyses of these flows. We now summarize some the key results. When $Fr \to \infty$, Ritter (1892) was the first to analyse dam-break flows from a lock of infinite length. The absence of a rear wall at the end of the lock and the uniform initial conditions mean that throughout the entire flow one of the characteristic variables remains constant and the motion is given by an expansion fan, centred at the lock gate. For a lock of finite length, we find that the interior dynamics are modified. There is a reflection from the rear wall that propagates forward. However when $Fr \to \infty$ this reflection does not reach the front and the frontal speed is not modified from the dam-break result given by Ritter (1892).

When Fr is finite, the initial expansion fan is preceded by a uniform region and the rear-wall reflection does catch up with the front. Differences in the ensuing motion then arise depending on the magnitude of Fr relative to 2. For $Fr < 2$, forward-propagating characteristics are reflected from the front and may propagate back to the rear wall, before being reflected forwards again. This phenomenon of a wave-like disturbance with successive reflections continues throughout the entire motion. For $Fr > 2$ the characteristics reflected from the front are unable to propagate back to the rear wall. Instead they remain localized to the front and eventually at relatively late times lead to the formation of a shock, over which the velocity and height fields are discontinuous. This behaviour has a complicated structure in the hodograph plane: the plane develops a 'fold' at $\beta = \beta_m$ and then there is a 'tear' when the shock is formed, as α and β jump discontinuously. Nevertheless, it is relatively straightforward to construct the entire solution, as demonstrated above. Finally for the transitional case, $Fr = 2$, the entire frontal region is associated with the characteristic value $\beta = 0$ and neither shocks nor successive reflections are found.

It is intriguing to compare these solutions and their structures in the hodograph and characteristic planes with similarity solutions for gravity current flows of a constant volume (Fannelop & Waldman 1972; Hoult 1972; Gratton & Vigo 1994). It has been shown that these similarity solutions are linearly stable (Grundy & Rottman 1985; Mathunjwa & Hogg 2006) and there is numerical evidence to suggest that they form the intermediate asymptotics for gravity current motion, modelled by the shallow water equations from lock-release initial conditions (Hogg, Ungarish & Huppert 2000). Gratton & Vigo (1994) report different forms of the solution, depending on whether Fr is less than or exceeds 2. Here we may readily demonstrate this in terms of the hodograph variables. The governing equation is given (2.13) with the boundary condition at the front given by (2.17). In line with many similarity solutions, we do not apply lock-release initial conditions, but merely demand that the volume of the current is constant, which in dimensionless variables is given by

$$\int_{x_r}^{x_N} h \, \mathrm{d}x = 1, \tag{5.1}$$

where x_r is the rear of the current. If the current remains attached to the rear wall then $x_r = 0$ and $u(x_r, t) = 0$, which is applied in the hodograph plane at $\alpha + \beta = 0$. Conversely if the back of the current moves away from the rear wall then $h(x_r, t) = 0$, which corresponds to $\alpha = \beta$ in the hodograph plane. First we note that the governing equation and frontal boundary condition are satisfied if

$$t = \frac{A}{|\alpha\beta|^{3/2}} + B, \tag{5.2}$$

where A and B are real-valued constants. For similarity solutions we set $B = 0$ because there cannot be an externally imposed time scale. The characteristic variable α is always positive, but β could potentially range over positive and negative values. When $Fr < 2$, $\lambda > 0$ and this means that the frontal boundary condition is applied to a negative value of β. Thus we may only apply the condition at the rear wall, $\beta = -\alpha$, and after enforcing (5.1) find

$$t = \frac{4(4 - Fr^2)^{3/2}}{Fr(6 - Fr^2)} \frac{1}{(-\alpha\beta)^{3/2}} \quad \text{and} \quad x = \tfrac{3}{4}(\alpha + \beta)t. \tag{5.3}$$

Conversely if $Fr > 2$, $\lambda < 0$ then the frontal boundary condition is applied to a positive value of β. Thus we may only apply the condition at the moving rear point, $\beta = \alpha$, and after enforcing (5.1) find

$$t = \frac{4(4 - Fr^2)^{3/2}}{Fr\big(6 - Fr^2[1 - (1 - 4/Fr^2)]^{3/2}\big)} \frac{1}{(\alpha\beta)^{3/2}} \quad \text{and} \quad x = \tfrac{3}{4}(\alpha + \beta)t. \tag{5.4}$$

The intermediate case, $Fr = 2$, is degenerate and corresponds to

$$x = \tfrac{3}{4}\alpha t \quad \text{and} \quad \beta = 0. \tag{5.5}$$

These similarity solutions represent the motion of gravity currents with a constant volume after a sufficient period so that initial conditions have become insignificant, apart from the specification of the total volume released. We expect, therefore, that they will represent the solutions from lock-release initial conditions in the regime $\alpha, |\beta| \ll 1$. We note that the analytical framework and solutions developed in this study may offer an opportunity to investigate in detail how flows approach a self-similar regime from given initial conditions, without the need for numerical computations. This may be a fruitful area for subsequent research.

There have been many laboratory realizations of gravity current flows generated from lock-release initial conditions (see, for example, Huppert & Simpson 1980; Rottman & Simpson 1983; Lowe *et al.* 2004). Rottman & Simpson (1983) demonstrated that during the slumping phase, the front moved at a constant velocity until it was caught up by a wave from the rear of the current, which arose from the reflection of the initial rearward-propagating rarefaction. Thereafter the front no longer moved at a constant speed, but decelerated and approached a self-similar state. These observations are in qualitative agreement with the phenomena predicted by this study. Rottman & Simpson (1983) find that the bore catches the front after 10 lock lengths; the present theory does not concur with this result, presumably because the experimental flows were generated from locks that were of the same depth as the ambient fluid. This means that the initial motion of the ambient cannot be neglected and so the use of a single-layer shallow water model may not capture quantitatively these experimental observations. This study has identified novel features of gravity current flow, such as successive reflections of waves along the length of the

current when $Fr < 2$ and shock formation at late times when $Fr > 2$. These have not yet been identified in laboratory experiments, the focus of which has usually been measurements of the speed and flow structure at the front, or the motion during relatively short times. However it would be of considerable interest to explore these new phenomena experimentally.

Finally we observe that hodograph transformations and analysis similar to that developed here may be useful for other flow scenarios. For example it is possible to derive similar governing equations in the hodograph plane for drag-free inertial flows on slopes, and the investigation of how these flows develop from prescribed initial conditions is another interesting topic for future research.

Appendix

In this Appendix we demonstrate that $x_1(-\beta_m) = 0$ provided $Fr < 2$. The calculation follows from (3.14); after rewriting the hypergeometric function $B(2, -2; \alpha, \beta)$ in terms of a Legendre function of order $\frac{1}{2}$ and integrating by parts we find that $x_1(-\beta_m) = f(-\beta_m)$, where f is defined by

$$f(\beta) \equiv 1 - \frac{2}{(-2\beta)^{1/2}} P_{1/2}\left(\frac{-4 - \beta^2}{4\beta}\right) + \frac{4}{(4 - \beta^2)^{1/2}} \int_1^{-(\beta^2+4)/(4\beta)} \frac{P_{1/2}(x)}{(\beta + 2x)^{1/2}} \, \mathrm{d}x. \quad \text{(A 1)}$$

We note that $f(-2) = 0$; this follows because the $\beta = -2$ characteristic from the front of the lock gate intersects the wall at $t = 1$, or alternatively, one may evaluate f directly from (A 1) as $\beta \to -2$. Further we note that this expression becomes unbounded as $\beta \to 0$ and may only be evaluated for $\beta < 0$. Next we find that

$$\frac{\mathrm{d}f}{\mathrm{d}\beta} = \frac{1}{(-2\beta^3)^{1/2}} P_{1/2}\left(\frac{-4 - \beta^2}{4\beta}\right) - \frac{4 - \beta^2}{(-2\beta)^{1/2} 2\beta^2} P'_{1/2}\left(\frac{-4 - \beta^2}{4\beta}\right)$$

$$+ \frac{4}{(4 - \beta^2)^{1/2}} \int_1^{-(\beta^2+4)/(4\beta)} \frac{-P_{1/2}(x)}{2(\beta + 2x)^{3/2}} + \frac{4\beta}{(4 - \beta^2)^{3/2}} \int_1^{-(\beta^2+4)/(4\beta)} \frac{-P_{1/2}(x)}{(\beta + 2x)^{1/2}}$$

$$+ \frac{(-2\beta)^{1/2}}{(\beta^2)} P_{1/2}\left(\frac{-4 - \beta^2}{4\beta}\right), \quad \text{(A 2)}$$

where $P'_{1/2}$ denotes the derivative of the Legendre function. This expression may be simplified by noting the following identity:

$$\int_1^{-(\beta^2+4)/(4\beta)} \left(\frac{\beta}{2(\beta + 2x)^{1/2}} - \frac{4 - \beta^2}{4(\beta + 2x)^{3/2}}\right) P_{1/2}(x) \, \mathrm{d}x$$

$$= \left[-(1 - x^2)(\beta + 2x)^{1/2}\left(P'_{1/2} - \frac{P_{1/2}}{\beta + 2x}\right)\right]_1^{-(\beta^2+4)/(4\beta)}. \quad \text{(A 3)}$$

Then substituting this identity into (A 2), we find that

$$\frac{\mathrm{d}f}{\mathrm{d}\beta} = 0. \quad \text{(A 4)}$$

Using $f(-2) = 0$, we then deduce that $f(\beta) = 0$, provided $\beta < 0$ and hence $x_1(-\beta_m) = 0$, provided $Fr < 2$.

REFERENCES

ABBOTT, M. B. 1961 On the spreading of one fluid over another: part 2. *La Houille Blanche* **6**, 827–836.

ARFKEN, G. B. & WEBER, H. J. 1995 *Mathematical Methods for Physicists*, Ed IV. Academic.

BENJAMIN, T. B. 1968 Gravity currents and related phenomena. *J. Fluid Mech.* **31**, 209–248.

BONNECAZE, R. T., HUPPERT, H. E. & LISTER, J. R. 1993 Particle-driven gravity currents. *J. Fluid Mech.* **250**, 339–369.

CARRIER, G. F. & GREENSPAN, H. P. 1957 Water waves of finite amplitude on a sloping beach. *J. Fluid Mech.* **1**, 97–109.

CARRIER, G. F., WU, T. T. & YEH, H. 2003 Tsunami run-up and draw-down on a plane beach. *J. Fluid Mech.* **475**, 79–99.

FANNELOP, T. K. & WALDMAN, G. D. 1972 Dynamics of oil slicks. *AIAA J.* **10**, 506–510.

GARABEDIAN, P. R. 1986 *Partial Differential Equations*. Chelsea Publishing.

GRATTON, J. & VIGO, C. 1994 Self-similar gravity currents with variable inflow revisited: plane currents. *J. Fluid Mech.* **258**, 77–104.

GROBELBAUER, H. P., FANNELOP, T. K. & BRITTER, R. E. 1993 The propagation of intrusion fronts of high density ratios. *J. Fluid Mech.* **250**, 669–687.

GRUNDY, R. E. & ROTTMAN, J. W. 1985 The approach to self-simiilarity of the solutions representing gravity current releases. *J. Fluid Mech.* **156**, 39–53.

HALLWORTH, M. A., HOGG, A. J. & HUPPERT, H. E. 1998 Effects of external flow on compositional and particle gravity currents. *J. Fluid Mech.* **359**, 109–142.

HÄRTEL, C., MEIBURG, E. & NECKER, F. 2000 Analysis and direct numerical simulation of the flow at a gravity-current head. Part 1. Flow topology and front speed for slip and np-slip boundaries. *J. Fluid Mech.* **418**, 189–212.

HOGG, A. J., HALLWORTH, M. A. & HUPPERT, H. E. 2005 On gravity currents driven by constant fluxes of saline and particle-laden fluid in the presence of a uniform flow. *J. Fluid Mech.* **539**, 349–385.

HOGG, A. J. & PRITCHARD, D. 2004 The effects of drag on dam-break and other shallow inertial flows. *J. Fluid Mech.* **501**, 179–212.

HOGG, A. J., UNGARISH, M. & HUPPERT, H. E. 2000 Particle-driven gravity currents: asymptotic and box-model solutions. *Eur. J. Mech.* **338**, 139–165.

HOULT, D. P. 1972 Oil spreading on the sea. *Annu. Rev. Fluid Mech.* **2**, 341–368.

HUPPERT, H. E. & SIMPSON, J. E. 1980 The slumping of gravity currents. *J. Fluid Mech.* **99**, 785–799.

VON KÁRMÁN, T. 1940 The engineer grapples with nonlinear problems. *Bull. Am. Math. Soc.* **46**, 615–683.

KERSWELL, R. R. 2005 Dam break with Coulomb friction: A model for granular slumping? *Phys. Fluids* **17**, 057101(1–16).

KLEMP, J. B., ROTUNNO, R. & SKAMAROCK, W. C. 1994 On the dynamics of gravity currents in a channel. *J. Fluid Mech.* **269**, 169–198.

LAUBER, G. & HAGER, W. H. 1998 Experiments to dambreak wave: Horizontal channel. *J. Hydr. Res.* **36**, 291–307.

LOWE, R. J., ROTTMAN, J. W. & LINDEN, P. F. 2004 The non-Boussinesq lock-exchange problem. Part 1. Theory and experiments. *J. Fluid Mech.* **537**, 101–124.

MATHUNJWA, J. S. & HOGG, A. J. 2006 Stability of gravity currents generated by finite-volume releases. *J. Fluid Mech.* **562**, 261–278.

PEREGRINE, D. H. 1972 Equations for water waves and the approximations behind them. In *Waves on Beaches and Resulting Sediment Transport* (ed. R. Meyer), Chapter 3, pp. 95–121. Academic.

PRITCHARD, D. & HOGG, A. J. 2005 On the transport of suspended sediment by a swash event on a plane beach. *Coastal Engng* **52**, 1–23.

RITTER, A. 1892 Die Fortpflanzung der Wasserwellen. *Z. Verein. Deutsch. Ing.* **36**(33), 947–954.

ROTTMAN, J. W. & SIMPSON, J. E. 1983 Gravity currents produced by instantaneous releases of heavy fluid in a rectangular channel. *J. Fluid Mech.* **135**, 95–110.

SHIN, J. O., DALZIEL, S. B. & LINDEN, P. F. 2004 Gravity currents produced by lock exchange. *J. Fluid Mech.* **521**, 1–34.

STANYUKOVICH, K. P. 1960 *Unsteady Motion of Continuous Media.* Pergamon.

UNGARISH, M. 2005 Dam-break release of a gravity current in a stratified ambient. *Eur. J. Mech.* B *(Fluids)* **24**, 642–658.

UNGARISH, M. & ZEMACH, T. 2005 On the slumping of high Reynolds number gravity currents in two-dimensional and axisymmetric configurations. *Eur. J. Mech.* B *(Fluids)* **24**, 71–90.

WHITHAM, G. B. 1974 *Linear and Nonlinear Waves.* Wiley.